Electronic and structural reconstructions of the polar (111) SrTiO₃ surface

X. Torrelles,[1] G. Cantele,[2] G. M. De Luca,[3,2] R. Di Capua,[3,2] J. Drnec,[4] R. Felici,[5] D. Ninno,[3,2] G. Herranz,[1] and M. Salluzzo[2]

[1]*Institut de Ciència de Materials de Barcelona (ICMAB-CSIC), Campus UAB, 08193 Bellaterra, Catalonia*
[2]*CNR-SPIN, c/o Complesso di Monte S. Angelo, via Cinthia, 80126 Napoli, Italy*
[3]*Dipartimento di Fisica, Università di Napoli "Federico II", Complesso di Monte S. Angelo, via Cinthia, 80126, Napoli, Italy*
[4]*ESRF, Experimental Division, 71 Avenue des Martyrs, 38000 Grenoble*
[5]*CNR-SPIN, c/o Università di Roma Tor Vergata, Via del Politecnico 1, 00133 Roma, Italy*

Polar surfaces are known to be unstable due to the divergence of the surface electrostatic energy. Here we report on the experimental determination, by grazing incidence x-ray diffraction, of the surface structure of polar Ti-terminated (111) SrTiO₃ single crystals. We find that the polar instability of the 1×1 surface is solved by a pure electronic reconstruction mechanism, which induces out-of-plane ionic displacements typical of the polar response of SrTiO₃ layers to an electron confining potential. On the other hand, the surface instability can be also eliminated by a structural reconstruction driven by a change in the surface stoichiometry, which induces a variety of 3×3 (111) SrTiO₃ surfaces consisting in an incomplete Ti (surface)–O₂ (subsurface) layer covering the 1×1 Ti-terminated (111) SrTiO₃ truncated crystal. In both cases, the TiO₆ octahedra are characterized by trigonal distortions affecting the structural and the electronic symmetry of several unit cells from the surface. These findings show that the stabilization of the polar (111) SrTiO₃ surface can lead to the formation of quasi-two-dimensional electron systems characterized by radically different ground states which depend on the surface reconstructions.

I. INTRODUCTION

The discovery of a quasi-two-dimensional electron system (q2DES) at the interfaces between (001) SrTiO₃ (STO) single crystals and other transition metal oxides, like LaAlO₃ (LAO) [1], LaGaO₃ [2], LaVO₃ [3], and LaTiO₃ [4], renewed the interest in the study of the electronic and structural properties of STO surfaces and related heterostructures. In these oxides, the charged planes stacked on top of a TiO₂ terminated (001) STO surface form a net dipole moment, giving rise to a divergence of the electrostatic surface energy. This well-known problem is commonly referred to as the "polarization catastrophe." In (001) LAO/STO, the polarization catastrophe can be avoided by an electronic reconstruction taking place alternatively or in addition to classical structural reconstructions. The consequent insulator-to-metal transition has a direct impact on atomic-scale structural lattice distortions across the (001) LAO/STO interface as shown in Refs. [5,6]. Beyond the electronic reconstruction, other mechanisms can induce the formation of a q2DES. In this respect special attention deserves the role of defects like oxygen vacancies, believed to be at the origin of the q2DES at the (001) STO surface [7,8], and the role of surface/interface stoichiometry, which theoretically can solve the polarization catastrophe problem also in (001) LAO/STO [9,10].

Besides (001) STO and LAO/STO, more recently scientists explored the properties of polar (111) heterostructures, which can also host a q2DES [11–13]. The stacking of atomic layers in (111) STO consists of alternating Ti and SrO₃ sheets [Figs. 1(a) and 1(b)]. In the ionic limit, where Ti, Sr, and O ions have nominal Ti⁴⁺, Sr²⁺, and O²⁻ charges, the (111) STO

surface is classified as a type-III polar surface [14,15]. Due to the strong polarity, the stability of an ideal Ti-terminated 1×1 (111) STO is debated, as it requires either a change of surface composition through adsorbates [16], surface reconstructions, or an electronic reconstruction.

(111) STO surfaces were previously investigated by atomic resolved scanning tunneling microscopy (STM) [17–19] and high-resolution transmission electron microscopy (HRTEM) [20,21]. Several kinds of reconstructions, including 3×3, 4×4, 5×5, 6×6, and even more complex ones [22] were identified on samples treated by Ar ion sputtering, and annealed in ultrahigh vacuum (UHV) or in oxygen atmosphere, for which there is no report of a q2DES at their surfaces or at the interface with LaAlO₃. More recently, a Ti-terminated 1×1 (111) STO surface was reported in the case of single crystals treated using a recipe similar to the Kawasaki etching used to get a Ti-terminated (001) STO [23,24]. This procedure consists of a chemical etching, using a buffered hydrofluoridric acid (BHF) solution, and annealing in flowing atmospheric pressure of O₂ at 950 °C [25]. The BHF method of preparation creates a Ti-terminated surface, which is known to be crucial for the formation of a q2DES at the (111) STO surfaces and at the interface with LaAlO₃ [11]. However, the experimental surface structure of these single crystals is not reported in the literature.

Besides the formation of a q2DES in (111) STO heterostructures, the study of polar (111) heterostructures is attractive because of the theoretical prediction of unexpected phenomena, like nontrivial topological states and quantum Hall effect up to room temperature [26]. In particular, a massive symmetry breaking was predicted in the case of (111)
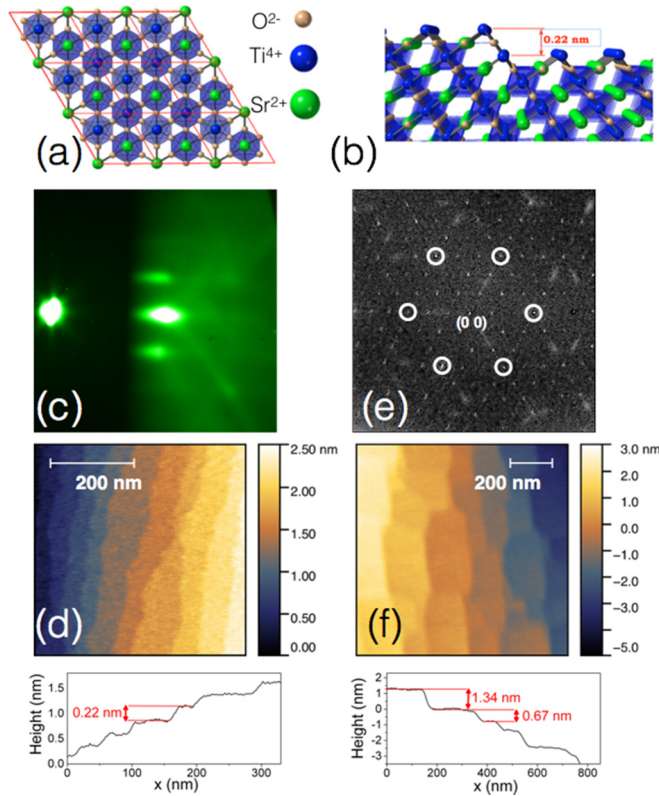
FIG. 1. (a) Top view of the 1×1 Ti-terminated (111) STO surface. (b) Lateral view of a stepped surface characterized by alternating terraces which are Ti terminated. The distance between two consecutive Ti layers is about 0.22 nm. (c) RHEED image of a 1×1, unreconstructed, (111) STO. The incoming 30-keV electrons impinge at grazing angles with a direction parallel to the steps. The diffraction spots correspond to the $[1\,1\,{-}2]$ in-plane distance (in the cubic indexing units). (d) Noncontact AFM topography of the 1×1 (111) STO surface and corresponding line profile across the steps (bottom panel). (e) SPA-LEED image taken on a 3×3 reconstructed (111) STO at 142 eV of incoming energy. Integer order diffraction spots are indicated by white circles. (f) Noncontact AFM topography of the 3×3 (111) STO surface and line profile (bottom) showing the presence of step heights equal or multiples of 0.676 nm.

LAO/STO quantum wells, with ordering of the titanium $3d$ orbitals (a_{1g}, e_g^π) derived bands depending on the strain and on the confinement [27]. One of the crucial ingredients for the realization of these unconventional ground states is a change of the bulk D_{4h} crystal field of the TiO_6 octahedra to a trigonal one, not only at the surface, where the structural symmetry is naturally broken, but also in the inner layers where the q2DES is located [28].

Motivated by these results, here we report a detailed study of the surface structure of Ti-terminated (111) SrTiO$_3$ crystals, prepared by a combination of chemical etching and high-temperature annealing, which exhibit a q2DES at their surfaces. We demonstrate an electronic reconstruction in the case of stoichiometric 1×1 surface of (111) STO crystals and a structural reconstruction in the case of Ti-rich surfaces exhibiting an unreported 3×3 surface lattice. The 3×3 reconstruction consists in an ordered $(TiO_2)_{1/3}$ layer on top of the 1×1 Ti-terminated (111) STO, and hosts a q2DES only

after annealing in UHV which introduces oxygen vacancies at the surface. Moreover, we find that in both cases several layers, in the same region where the q2DES resides, are characterized by trigonal distortions which depend on the surface reconstruction and can drive different kinds of unconventional ground states.

II. EXPERIMENTAL RESULTS

All the (111) SrTiO$_3$ single crystals studied in this work were prepared by buffered hydrofluoric acid (BHF, NH4F:HF 87.5:12.5, pH 5.5) chemical etching and subsequent high-temperature oxygen annealing [23–25]. The surface structure was studied by UHV spot profile analysis low-energy electron diffraction (SPA-LEED), reflection high-energy electron diffraction (RHEED), atomic force microscopy (AFM), STM, and grazing incidence surface x-ray diffraction (SXRD). In Figs. 1(c)–1(f) we show typical RHEED, SPA-LEED, and AFM data on BHF etched (111) STO surfaces. Single crystals annealed in O$_2$ flow at 950 °C show a 1×1 RHEED diffraction pattern [Fig. 1(c)] and a surface composed by alternating terraces (widths of the order of 50 nm or less) with heights of 0.22 nm [Fig. 1(d)], corresponding to the distance between two consecutive Ti layers [Fig. 1(b)]. On the other hand, (111) STO single crystals annealed at temperatures between 1050 and 1200 °C exhibit a 3×3 reconstructed surface, as shown by the SPA-LEED diffraction pattern in Fig. 1(e). Their surfaces reveal much wider terraces (up to 200 nm width) with step heights compatible with the distance between two unit cells along the (111) direction, $c = 0.676\,37$ nm, or multiples [Fig. 1(f)].

SXRD experiments were performed in UHV and at room temperature at the ID03 beamline of the European Synchrotron Research Facility. Crystal truncation rod (CTR) and fractional order rod (FOR) data, i.e., the profile along the direction perpendicular to the surface (L) of the structure factor, F_{HKL}, were acquired using a two-dimensional (2D) Maxipix detector and a 24-keV x-ray beam. The large data sets were corrected and integrated using the data reduction and analysis software BINocular developed at the ID03 of ESRF [29]. The structural refinement was performed using the program ROD [30], by fitting simultaneously, for each sample, several nonequivalent CTRs, and FORs in the case of reconstructed surfaces, following the method of Ref. [31]. The models used were built on the basis of the (111) SrTiO$_3$ cell within the $p3m1$ space group (with $a = b = 0.552$ nm, $c = 0.676\,37$ nm, $\alpha = \beta = 90°$, $\gamma = 120°$). For the 1×1 structure, we used eight inequivalent CTR's corresponding to 2332 F_{HKL} structure factor points. For the 3×3 reconstructed surface, we acquired a total of 7513 reflections which reduced to 5420 after averaging between the equivalent reflections involving 12 FORs and 15 CTRs.

First we discuss the simpler 1×1 surface structure. Ideal SrO$_3$, titanium [Fig. 2(a), blue lines], or mixed terminated surfaces do not provide good solutions of the experimental data. However, for the Ti-terminated surface model, the χ^2 factor reduces down to about 2.0 after letting the atomic positions to relax up to four unit cells along the surface normal and allowing possible in-plane relaxations. Further improvement of the data fitting requires us to explicitly take into account the
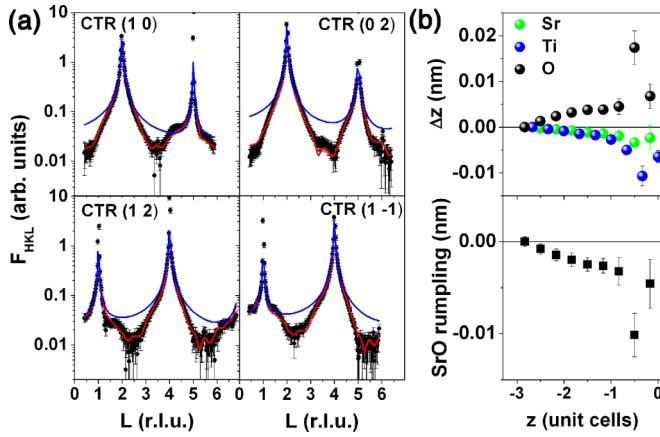
FIG. 2. (a) CTR data vs L (in reciprocal-lattice units, r.l.u., of the $p3m1$ unit cell) for the 1×1 (111) STO surface (scatter black squares), the ideal Ti-terminated model calculations (blue lines, $\chi^2 = 6.18$), and the two terraces Ti-terminated fit (red lines, $\chi^2 = 1.0$). (b) Upper panel: displacements along the surface normal, with respect to the bulk, of Sr, Ti, and O ions as function of the z coordinate in $p3m1$ units ($z = 0$ is the surface); lower panel: rumpling of the SrO_3 planes, defined as $(z_{Sr} - z_O)/2$, i.e., half of the distance between Sr and oxygen planes.

peculiar terrace structure of the surface shown in Figs. 1(b) and 1(d). Since the terraces are less than 50 nm wide [see Fig. 1(d)], the scattered x rays coherently interfere resulting in distinctive truncation rod profiles. Thus the data can be very well reproduced by a two-terrace, Ti terminated, model [Fig. 2(a), red line] [32], which gives the best reduced χ^2 of the order of 1.0 and an R factor $= \sum |F_{calc} - F_{exp}|/\sum F_{exp}$ of 19%. It is worth noting that the two-terrace model does not increase the number of free parameters, since we use the same displacements for equivalent ions in each of the two terraces [33]. Interestingly, according to the refined model, the surface layers exhibit substantial ionic relaxations extending up to three unit cells from the surface (i.e., about 2.5 nm), consistent with the formation of a confined electron doped q2DES. In particular, we find that the cations relax towards the bulk [Fig. 2(b), upper panel] and the SrO_3 layers get substantially rumpled [Fig. 2(b), bottom panel], because the negative charged oxygen ions move out from the Sr planes towards the surface. These ionic displacements are typical of the polar response of STO as a consequence of the presence of an electric field confining electrons [5]. The results are in qualitative agreement with *ab initio* theoretical calculations [34,35], although the experimentally refined structure shows lower distortions possibly due to the screening effect of localized and delocalized charge carriers not captured by theory.

The out-of-plane ionic relaxations found are sufficiently large to trigonally distort the TiO_6 octahedral cages [36]. This observation has profound effects on the electronic properties of the system, as it implies that the crystal field has a trigonal symmetry for several layers starting from the surface. In particular, the trigonal axis (i.e., the c axis in $p3m1$ symmetry) is compressed (up to -0.25%), corresponding to a lowering of the a_{1g} derived band's energy with respect to the e_g^{π} one. A qualitatively similar band splitting was recently found for the

q2DES formed in conducting (111) LAO/STO, as shown in Ref. [28].

In order to analyze the more complex 3×3 reconstructed surface, we considered different possible structural models. First, we examined a 3×3 lattice ($a = b = 1.656$ nm, $c = 0.67637$ nm) terminated by an incomplete, ordered, SrO_3 and/or Ti layers, following the natural bulk sequence. However, these models are unable to fit the experimental data (reduced $\chi^2 > 3.5$). On the other hand, a very good fit is obtained using the model described in Fig. 3 (reduced $\chi^2 = 1.1$, R factor of 15.6%). Starting from an ideally Ti-terminated surface, we add a complete oxygen layer and on top a Ti overlayer [Figs. 3(a) and 3(b)]. Furthermore, we introduce occupation parameters for the subsurface oxygen and surface titanium ions. In the initial model each surface Ti ion is coordinated to three oxygen ions. The final fit converges to a 1/3 occupation of each Ti ion on the surface and to a 1/4 occupation of the oxygen ions in the second layer. As a consequence each topmost Ti ion is coordinated in average with two, instead of three, oxygen ions, which ensures charge neutrality but results in a configurational disorder of the subsurface ions. The solution can be understood as the coherent superposition of three Ti-O_2 sublattices, labeled with numbers 1–3 in Fig. 3(b), each of them forming a 3×3 lattice.

Additionally, we find substantial displacements of the ions from the ideal bulk positions, inducing again trigonal distortions of the TiO_6 octahedra [36]. The trigonal axis is again compressed with respect to the bulk value (up to -1.1% in the first unit cell below the surface). However, both oxygen and cations relax towards the bulk and the rumpling of SrO_3 is opposite to the 1×1 case, i.e., opposite to the one expected in the case of a screening of an electron confining potential, thus inconsistent with an electronic reconstruction.

The structural model shown in Fig. 3 differs from other 3×3 structures reported in the literature, in particular from the one recently reported in Ref. [22] on (111) STO surfaces prepared by Ar sputtering and high-temperature annealing. The 3×3 model of Ref. [22] consists in ordered tetrahedral TiO_4 units positioned on top of octahedral TiO_5 units. As shown in Fig. S1 of the Supplemental Material [36], a fit of the diffraction data with the model proposed in Ref. [22] shows large discrepancies for all fractional rods, with a χ^2 value of 1.8 and an R factor of 37%, much larger than the one obtained with the model reported here. The two 3×3 structures found in the present work and in Ref. [22] are then quite different. In particular, the overall Ti/Sr ratio of the surface unit cell is in our case 1.33, lower than the value of 1.66 reported in Ref. [22]. We attribute the observed differences to a larger excess of Ti created at the surface by Ar sputtering.

We find that the 3×3 reconstruction found in this work is rather stable and it does not show the formation of a q2DES without additional treatments. In particular, we find that the 3×3 surface reconstructions, studied by measuring the FORs profiles, is not substantially modified during *in situ* thermal treatments either in vacuum ($P < 10^{-8}$ mbar) and in oxygen flow [$P(O_2) = 10^{-5}$ mbar] up to a temperature of $700\,°C$.

However, annealing in UHV can introduce oxygen vacancies at the surface and the formation of a q2DES. In Fig. 4 we show *in situ* I-V and dI/dV local STM spectroscopy data on the 3×3 (111) STO surface annealed in UHV at
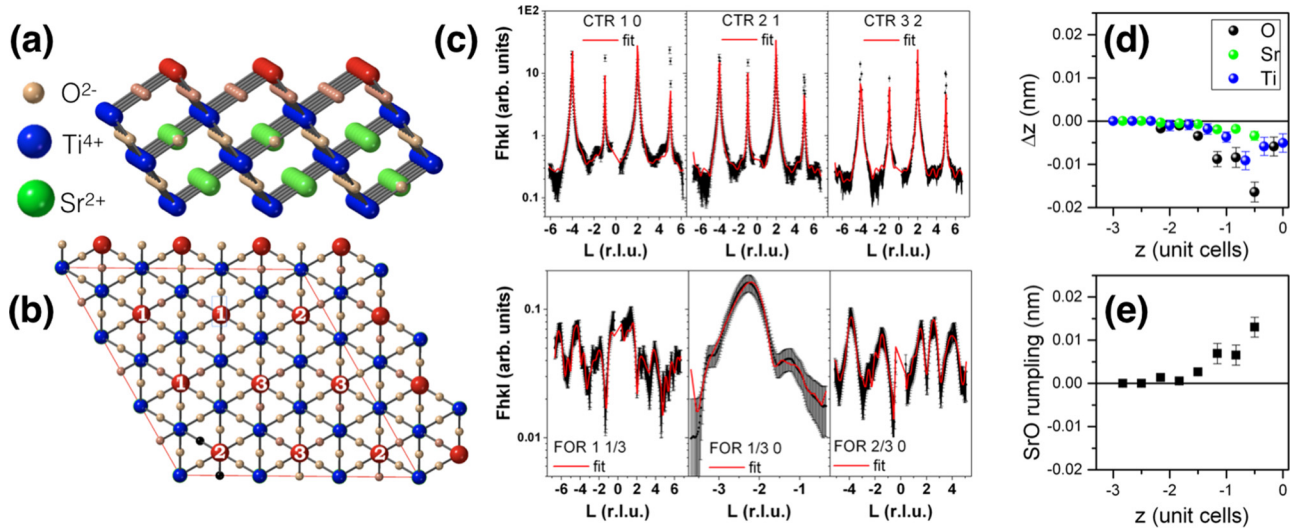
FIG. 3. (a) Lateral and (b) top view of the initial average surface model used to fit the diffraction data on the 3×3 reconstructed STO (111) surface. On top of a Ti-terminated ideal truncated crystal, we add a complete oxygen layer and a complete titanium layer (topmost Ti^{4+} ions are denoted with red spheres). Occupational parameters for the top Ti and oxygen ions are added to the model. The average model in (b) can be considered as the superposition, with equal 33% occupancy, of the three 3×3 lattices formed by the TiO_2 units labeled 1, 2, and 3, respectively. (c) Comparison between experimental (black circles) and calculated (red lines) CTRs and FORs vs L (in reciprocal-lattice units, r.l.u., of the $p3m1$ unit cell). (d) Average displacements along the surface normal, with respect to the bulk, of the Sr, Ti, and O ions as function of the z coordinate in lattice units ($p3m1$ space group; $z = 0$ is the surface). (e) Rumpling of the SrO_3 planes.

$250\,^{\circ}C$ for 12 h. While the surface morphology is substantially unaffected by the additional low-temperature annealing, as shown by the STM image in Fig. 4(a), local spectroscopy demonstrates that the surface is conducting [Figs. 4(b) and 4(c)]. The low-temperature annealing procedure used does not create enough vacancies to induce bulk conductivity. In particular, as for the 1×1 surface, when exposed to ambient pressure, the 3×3 (111) STO becomes fully insulating.

In order to investigate the properties of the q2DES formed at this variety of 3×3 reconstructed (111) STO after low-temperature UHV annealing, we acquired a complete set of SXRD data and performed a structural refinement using the same model shown in Fig. 3. We find a reduction of the oxygen stoichiometry in the first layers ($<10\%$ oxygen vacancies) and a slight decrease of the trigonal compression (-0.7% instead of -1.1%). Thus the 2D electron system created is characterized again by a splitting between the a_{1g} and the e_g^{π} derived bands, and a trigonal compression larger than the

one estimated in the case of the 1×1 (111) STO surface. Thus, a larger trigonal crystal-field splitting is expected, which will have an impact on the electronic ground state of the system.

III. DISCUSSION

Our study reveals two fundamental reconstruction mechanisms, either electronic or structural, solving the polar instability of the polar Ti-terminated (111) STO surface. The ideal Ti-terminated surface is strongly polar and in the ionic limit has a charge of $+4e$/unit cell (e is the electron charge). Even taking into account the covalent character of the Ti-O (and Sr-O) bonds, the Ti and SrO_3 layers are characterized by a net charge $\sigma_B = \pm 2.25e$/unit cell [34]. Thus the stability of this system requires a compensation mechanism. Here, the large electric field induced by the charged layers can be only compensated by a transfer of electrons from SrO_3 to the
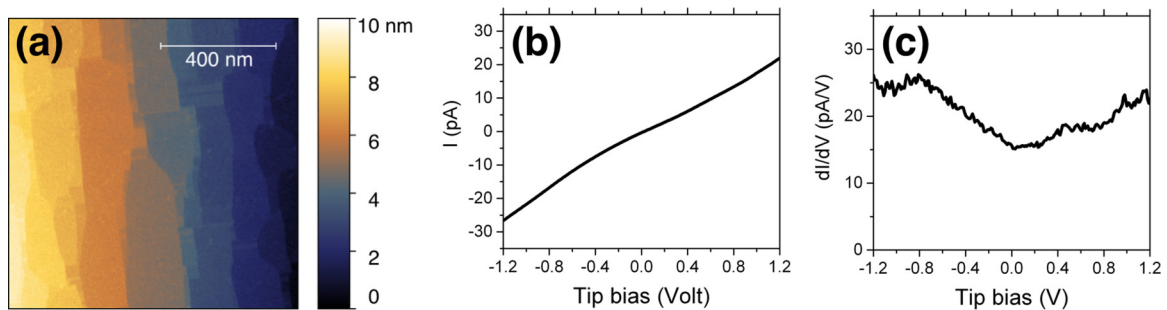

FIG. 4. (a) *In situ* scanning tunneling microscopy image on a 3×3 reconstructed (111) STO single crystal annealed in ultrahigh vacuum at $250\,^{\circ}C$ for 12 h. The image has been acquired in constant current mode with a tunneling current of 50 pA and a bias voltage on the tip (electrochemical etched iridium wire) of 1.0 V. (b) Typical tunneling current I and (c) differential conductance dI/dV vs bias-voltage characteristics demonstrating the metallic nature of the surface state.

Ti surface layer. According to theory [34,35], this electron transfer shows up as polar distortions and consequently as a rumpling of the planes within a finite region at the surface which gradually reduces to zero into the bulk [Fig. 2(b)]. In the rumpled region, the electrons transferred into Ti-3d states can form a q2DES. Thus the picture, emerging from the experimental data, is in good qualitative agreement with *ab initio* calculations [34,35]. It is worth noting that at room temperature the polar distortions are present within a thickness of about 2.5 nm from the surface, comparable to what is found in the case of LAO/STO (001) heterostructures [5]. However, the electronic reconstruction and the formation of a q2DES at the surface of (111) STO is metastable. Indeed, when the sample is exposed to air it becomes insulating. We conjecture that the disappearance of the q2DES is due to adsorbates on the surface which form at ambient pressures and compensate the surface polarity [16]. These adsorbates can desorb during x-ray irradiation in UHV, and the consequent surface polarity triggers an electronic reconstruction. X-ray irradiation can also promote oxygen vacancies at the surface [13], however, while they are likely unavoidable defects, their creation is not the main mechanism of the realization of the q2DES in this case. Indeed, by introducing oxygen occupation parameters in our model the structural solution converges to a χ^2 less than 5% lower than the case of full oxygen occupation, and to an amount of oxygen vacancies between 2% an 5% in the first three unit cells unable to compensate the divergence of the electrostatic potential.

The structural reconstruction of (111) STO, solving the polar instability by creating a 3×3 lattice, is, on the other hand, rather stable. This can be explained by a full compensation of the electrostatic potential by the Ti stoichiometry and surface reconstruction. The compensation of the electrostatic potential takes place if the surface charge σ_s is equal to $\sigma_B/2$. In order to verify if this condition is effectively met, we recalculate the effective Bader charge of the surface Ti ions, considering both covalence and new surface coordination. Here, we use the bulk Bader charge values of Sr, Ti, and O ions estimated in Ref. [34], and in particular the σ_B value for the net charge associated to each (bulk) Ti ion. As a consequence, assuming the initial ionic valence of Ti is equal to $+4e$, the charge transfer between Ti and O ions (considering that in the bulk each Ti ion is coordinated to six O ions) is given by

$$\Delta_{\text{Ti-O}} = \frac{4 - 2.25}{6} e/\text{unit cell} = 0.29 e/\text{unit cell}. \quad (1)$$

In our model, the fit converges to an overall 1/3 occupation for the Ti ions on the surface, and therefore the net charge of this surface layer is given by

$$\sigma_S = \frac{\sigma_{\text{Ti}}^{(S)}}{3}/\text{unit cell}, \quad (2)$$

where $\sigma_{\text{Ti}}^{(S)}$ denotes the net charge of each Ti ion on the surface layer.

Assuming at the surface the same charge transfer between Ti and O ions of the bulk, and considering that each surface titanium is coordinated with two O ions, we can write

$$\frac{4e - \sigma_{\text{Ti}}^{(S)}}{2}/\text{unit cell} = 0.29 e/\text{unit cell}, \quad (3)$$
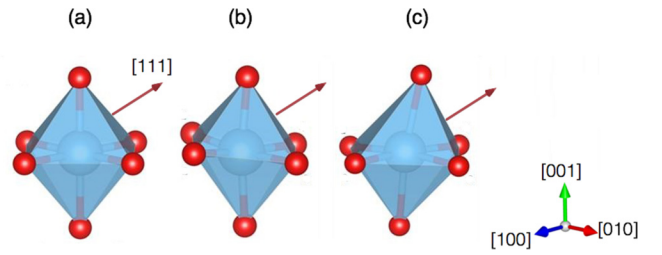

FIG. 5. Trigonal distortion of the first subsurface unit cell of the ideal TiO$_6$ octahedra (a) in the case of electronic reconstructed 1×1 (111) STO (b) and of structural reconstructed 3×3 (111) STO (c) hosting a quasi-two-dimensional electron gas. Red arrows indicate the [111] surface vector.

from which we infer $\sigma_S^{(S)} = 3.42e$, and therefore [from Eq. (2)] we find an effective surface charge of about $\sigma_S = +1.140e$/unit cell, which is very similar to $\sigma_B/2 = 1.125e$/unit cell. This very simple estimate shows that the bulk electrostatic potential is compensated at the 3×3 reconstructed surface by the change in the surface stoichiometry alone which does explain its stability.

IV. CONCLUSIONS

In this paper, we present a study of the surface structure, ionic relaxation, and lattice distortions of 1×1 and 3×3 (111) STO surfaces hosting a q2DES at their surfaces using a combination of different surface characterization techniques and in particular by the SXRD crystallography technique. We found that the compensation of the strong polarity of Ti-terminated (111) STO can be achieved either by a purely electronic reconstruction mechanism or by a structural reconstruction, depending on the surface stoichiometry, i.e., the Ti excess at the surface. In both cases, not only the surface but also several inner layers show trigonal distortions of the TiO$_6$ octahedra which depend quantitatively on the kind of surface structure and reconstruction realized. This result is summarized in Fig. 5, where we show a comparison between bulk and surface TiO$_6$ octahedra in the 1×1 and 3×3 (111) STO samples hosting a q2DES as obtained from the structural refinement. The trigonal distortions are the consequences of the out-of-plane and in-plane displacements of Ti and oxygen ions within at least three $p3m1$ unit cells from the (111) surface. As a consequence of these distortions, we found that 1×1 and 3×3 (111) STO surfaces realized by BHF etching and thermal annealing show a compression of the (111) trigonal axis of the unit cells where the q2DES resides. This has an impact on the electronic properties of system, which depend on the trigonal crystal-field splitting [26,27] and suggests a method towards a control of the symmetry and splitting of the q2DES in (111) surfaces and interfaces through a careful tuning of the chemical termination and stoichiometry which can induce different surface reconstructions.

[1] A. Ohtomo and H. Y. Hwang, Nature (London) **427**, 423 (2004).

[2] P. Perna, D. Maccariello, M. Radović, U. Scotti di Uccio, I. Pallecchi, M. Codda, D. Marrè, C. Cantoni, J. Gazquez, M. Varela, S. J. Pennycook, and F. Miletto Granozio, Appl. Phys. Lett. **97**, 152111 (2010).

[3] Y. Hotta, T. Susaki, and H. Y. Hwang, Phys. Rev. Lett. **99**, 236805 (2007).

[4] J. Biscaras, N. Bergeal, S. Hurand, C. Grossetête, A. Rastogi, R. C. Budhani, D. LeBoeuf, C. Proust, and J. Lesueur, Phys. Rev. Lett. **108**, 247004 (2012).

[5] M. Salluzzo, S. Gariglio, X. Torrelles, Z. Ristic, R. Di Capua, J. Drnec, M. M. Sala, G. Ghiringhelli, R. Felici, and N. B. Brookes, Adv. Mater. **25**, 2333 (2013).

[6] J. Gazquez, M. Stengel, R. Mishra, M. Scigaj, M. Varela, M. A. Roldan, J. Fontcuberta, F. Sánchez, and G. Herranz, Phys. Rev. Lett. **119**, 106102 (2017).

[7] R. Di Capua, M. Radović, G. M. De Luca, I. Maggio-Aprile, F. Miletto Granozio, N. C. Plumb, Z. Ristic, U. Scotti di Uccio, R. Vaglio, and M. Salluzzo, Phys. Rev. B **86**, 155425 (2012).

[8] A. F. Santander-Syro, O. Copie, T. Kondo, F. Fortuna, S. Pailhès, R. Weht, X. G. Qiu, F. Bertran, A. Nicolaou, A. Taleb-Ibrahimi, P. Le Fèvre, G. Herranz, M. Bibes, N. Reyren, Y. Apertet, P. Lecoeur, A. Barthélémy, and M. J. Rozenberg, Nature (London) **469**, 189 (2011).

[9] N. Pavlenko, T. Kopp, E. Y. Tsymbal, J. Mannhart, and G. A. Sawatzky, Phys. Rev. B **86**, 064431 (2012).

[10] L. Yu and A. Zunger, Nat. Commun. **5**, 5118 (2014).

[11] G. Herranz, F. Sánchez, N. Dix, M. Scigaj, and J. Fontcuberta, Sci. Rep. **2**, 758 (2012).

[12] T. C. Rödel, C. Bareille, F. Förtuna, C. Baumier, F. Bertran, P. Le Fèvre, M. Gabay, O. Hijano Cubelos, M. J. Rozenberg, T. Maroutian, P. Lecoeur, and A. F. Santander-Syro, Phys. Rev. Appl. **1**, 051002 (2014).

[13] S. McKeown Walker, A. de la Torre, F. Y. Bruno, A. Tamai, T. K. Kim, M. Hoesch, M. Shi, M. S. Bahramy, P. D. C. King, and F. Baumberger, Phys. Rev. Lett. **113**, 177601 (2014).

[14] P. W. Tasker, J. Phys. C **12**, 4977 (2001).

[15] A. Pojani, F. Finocchi, and C. Noguera, Surf. Sci. **442**, 179 (1999).

[16] M. Saghayezhian, L. Chen, G. Wang, H. Guo, E. W. Plummer, and J. Zhang, Phys. Rev. B **93**, 125408 (2016).

[17] H. Tanaka and T. Kawai, Surf. Sci. **365**, 437 (1996).

[18] B. C. Russell and M. R. Castell, Phys. Rev. B **75**, 155433 (2007).

[19] B. C. Russell and M. R. Castell, J. Phys. Chem. C **112**, 6538 (2008).

[20] A. N. Chiaramonti, C. H. Lanier, L. D. Marks, and P. C. Stair, Surf. Sci. **602**, 3018 (2008).

[21] L. D. Marks, A. N. Chiaramonti, F. Tran, and P. Blaha, Surf. Sci. **603**, 2179 (2009).

[22] L. D. Marks, A. N. Chiaramonti, S. U. Rahman, and M. R. Castell, Phys. Rev. Lett. **114**, 226101 (2015).

[23] M. Kawasaki, K. Takahashi, T. Maeda, R. Tsuchiya, M. Shinohara, O. Ishiyama, T. Yonezawa, M. Yoshimoto, and H. Koinuma, Science **266**, 1540 (1994).

[24] G. Koster, B. L. Kropman, G. J. Rijnders, D. H. Blank, and H. Rogalla, Appl. Phys. Lett. **73**, 2920 (1998).

[25] A. Biswas, P. B. Rossen, C. H. Yang, W. Siemons, M. H. Jung, I. K. Yang, R. Ramesh, and Y. H. Jeong, Appl. Phys. Lett. **98**, 051904 (2011).

[26] Di Xiao, W. Zhu, Y. Ran, N. Nagaosa, and S. Okamoto, Nat. Commun. **2**, 596 (2011).

[27] D. Doennig, W. E. Pickett, and R. Pentcheva, Phys. Rev. Lett. **111**, 126804 (2013).

[28] G. M. De Luca, R. Di Capua, E. Di Gennaro, A. Sambri, F. M. Granozio, G. Ghiringhelli, D. Betto, C. Piamonteze, N. B. Brookes, and M. Salluzzo, Phys. Rev. B **98**, 115143 (2018).

[29] J. Drnec, T. Zhou, S. Pintea, W. Onderwaater, E. Vlieg, G. Renaud, and R. Felici, J. Appl. Crystallogr. **47**, 365 (2014).

[30] E. Vlieg, J. Appl. Crystallogr. **33**, 401 (2000).

[31] A. Fragneto, G. M. De Luca, R. Di Capua, U. Scotti di Uccio, M. Salluzzo, X. Torrelles, T.-L. Lee, and J. Zegenhagen, Appl. Phys. Lett. **91**, 101910 (2007).

[32] From the data analysis we can exclude cation vacancies above 5% in the first three unit cells or the presence of an additional oxygen overlayer (even only partially populated).

[33] U. Magdans, H. Gies, X. Torrelles, and J. Rius, Eur. J. Mineral. **18**, 83 (2006).

[34] N. Sivadas, H. Dixit, V. R. Cooper, and D. Xiao, Phys. Rev. B **89**, 075303 (2014).

[35] Y. Yin, J. Wang, H. Zhu, K. Lv, and X. S. Wu, Vacuum **120**, 83 (2015).

[36] See Supplemental Material at http://link.aps.org/supplemental/10.1103/PhysRevB.99.205421 for a comparison between the experimental data and the 3×3 STO surface structure proposed in Ref. [22] (suppl. note 1 and Fig. S1), and for details concerning the structural distortions obtained from the data fitting shown in Fig. 5 and in Table S1.